Letter

Ballistic-to-diffusive transition in engineered counterpropagating quantum Hall channels

Aifei Zhang [1], Kenji Watanabe [2], Takashi Taniguchi [3], Patrice Roche [1], Carles Altimiras [1], François D. Parmentier [1,4], and Olivier Maillet [1,*]

[1] Université Paris-Saclay, CEA, CNRS, SPEC, 91191 Gif-sur-Yvette, France
[2] Research Center for Electronic and Optical Materials, National Institute for Materials Science, 1-1 Namiki, Tsukuba 305-0044, Japan
[3] Research Center for Materials Nanoarchitectonics, National Institute for Materials Science, 1-1 Namiki, Tsukuba 305-0044, Japan
[4] Laboratoire de Physique de l'Ecole normale supérieure, ENS, Université PSL, CNRS, Sorbonne Université, Université Paris Cité, F-75005 Paris, France

(Received 28 May 2025; revised 23 August 2025; accepted 14 October 2025; published 19 November 2025)

Exotic quantum Hall systems hosting counterpropagating edge states can show seemingly nonuniversal transport regimes, usually depending on the size of the sample. We experimentally probe transport in a quantum Hall sample engineered to host a tunable number of counterpropagating edge states. The latter are coupled by Landauer reservoirs, which force charge equilibration over a tunable effective length. We show that charge transport is determined by the balance of up- and downstream channels, with a ballistic regime emerging for unequal numbers of channels. For equal numbers, we observe a transition to a critical diffusive regime, characterized by a diverging equilibration length. Our approach allows simulating the equilibration of hole-conjugate states and other exotic quantum Hall effects with fully controlled parameters using well-understood quantum Hall states.

DOI: 10.1103/3d25-wpth

Quantum Hall (QH) insulators are characterized by a gapped, electrically insulating bulk, and conduction along their edge via a quantized number of one-dimensional chiral edge channels. In most cases, the edge channels copropagate; i.e., they have the same chirality. This leads to extremely robust transport properties, even in the presence of strong interactions between edge channels [1,2]: edge transport is then ballistic and dissipationless, and the Hall conductance is exactly given by $\nu e^2/h$, where e is the electron charge, h is Planck's constant, and $\nu = nh/eB$ is the filling factor characterizing the topology of the QH states (n is the carrier density and B is the perpendicular magnetic field). However, the edge channels can also be counterpropagating; this is notably the case of the quantum spin Hall (QSH) effect, which hosts two counterpropagating channels with opposite spin polarizations [3], but it is also expected for hole-conjugate states of the fractional quantum Hall (FQH) effect such as $\nu = 2/3$ [4]. There, Coulomb interactions and interchannel tunneling can lead to equilibration along the edge [5], drastically impacting transport properties, which become length-dependent. Theoretical [6–12] and experimental [13–18] investigations of charge and heat transport in hole-conjugate FQH states, combined with the general observation of imperfect conductance quantization in the QSH effect [3,19–24], point toward different transport regimes depending on the number of equilibrating edge channels and their respective conductances. If the overall upstream and downstream conductances are different, the transport can be ballistic, with a quantized conductance and negligible dissipation at large scale. If upstream and downstream conductances are equal, however, the transport becomes diffusive, with inexact conductance quantization and dissipation all along the edge. Remarkably, this applies to both charge and heat transport, which can lead to striking transport decoupling effects in FQH channels where the electrical conductance is fractional while the thermal conductance is integer [17,18,25].

Understanding and exploring the transition between the diffusive and ballistic regimes in equilibrating counterpropagating edge channels is an experimental challenge, as it requires controlling the number of equilibrating channels, the nature and strength of the equilibration process, and the ability to probe dissipation along the edge of the sample. Inspired by recent theoretical models [9,10,12], we have realized an experiment where counterpropagating integer quantum Hall (IQH) channels equilibrate through a series of Ohmic contacts (Landauer reservoirs) that provide both charge redistribution and energy equilibration between channels. Our approach presents multiple advantages, stemming from its simplicity: For any edge configuration among a wide range, we directly measure the voltage of the Ohmic contacts, yielding the voltage drop and dissipation along the edge, as well as the conductance and its length dependence. We emulate charge equilibration in a QH edge with tunable numbers of counterpropagating channels. This allows us to observe and fully explore the transition between the ballistic and diffusive regimes, in agreement with exact scattering formalism calculations.

Our experiment consists of two Hall bars [devices A and B; see Fig. 1(a)] made of monolayer graphene encapsulated in hexagonal boron nitride [26], each individually gated

*Contact author: olivier.maillet@cea.fr

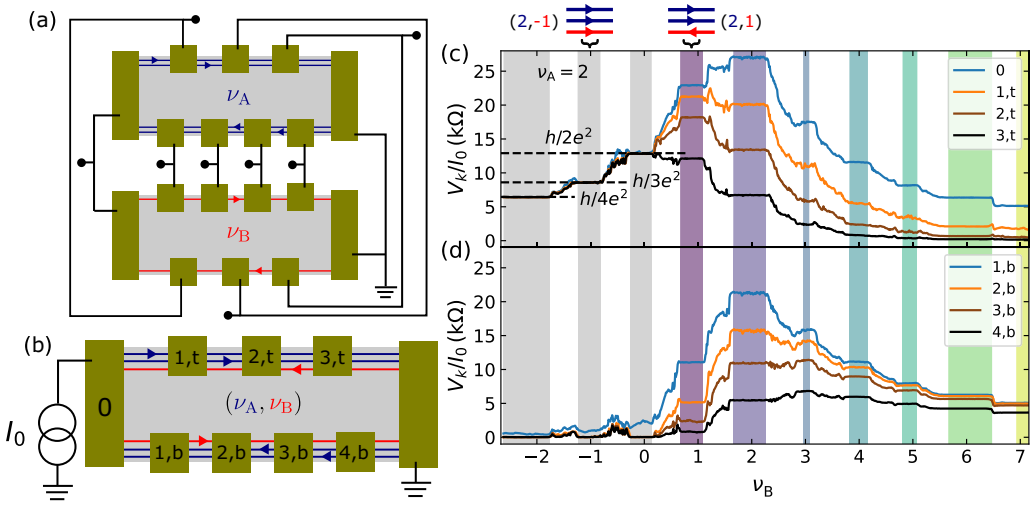

FIG. 1. (a) Schematics of the measured two-Hall bar device and paired contacts. (b) Effective Hall bar: equivalent configuration with counterpropagating edge channel numbers set by individual filling factors ν_A and ν_B. In this example, one pair of contacts (labeled 0 here) is connected to a current source (injection contact), and $N_t = 3$ and $N_b = 4$ intermediate contacts on the top and bottom edges, respectively, are left floating, acting as effective Landauer reservoirs. Example sweep of device B's gate voltage/density (in filling factor units ν_B) while keeping $\nu_A = 2$, for top [panel (c)] and bottom edge contacts [panel (d)]. The colors assigned to each plateau with $\nu_B > 0$ are used throughout the Letter.

by a graphite back gate. Both are cooled down to 10 mK under a 14 T perpendicular magnetic field. The Hall bars are connected in a top-to-tail fashion, such that the kth contact of device A, starting clockwise from the first contact next to the cold-grounded drain, is connected with the kth contact of device B, starting anticlockwise from the first contact next to the drain. Paired contacts share the same potential, and each pair may be left floating (while its voltage with respect to ground is measured), put to ground, or used for current injection. This implements an effective single Hall bar [Fig. 1(b)] with a tunable number of counterpropagating channels determined by the filling factor of each Hall bar $\nu_{A/B}$. By convention, we define the edge flowing from (resp. into) the injection contact, when running clockwise on the effective Hall bar, as the top (resp. bottom) edge, labeled "t" (resp. "b"). We introduce N_t (resp. N_b) the number of intermediate floating Ohmic contacts on the top (resp. bottom) edge. The gate-to-density correspondence of one device is determined by setting the other device at $\nu = 0$, thus ensuring that current flows only in the former (see the Supplemental Material [27]). We then keep device A at a fixed filling factor ν_A and tune the charge carrier density n_B of device B to obtain filling factors ranging from $\nu_B = -2$ to $\nu_B = 7$. We inject a low-frequency ($\approx$1 Hz) current through the source contacts of our choice in both devices and monitor voltages on each pair of contacts, including the source, through standard lock-in measurements. A sweep of the back gate of device B for $\nu_A = 2$ in the configuration of Fig. 1(b) is shown in Figs. 1(c) and 1(d). When device B is p-doped ($\nu_B < 0$), the voltage on the top effective edge ["t"-labeled contacts in Fig. 1(c)] remains constant and equal to that of the injection, while voltages on all bottom edge contacts remain zero, up to some residual backscattering observable on contact 1,b. This is expected since here, all channels copropagate, making our effective Hall bar behave like a regular one. On the contrary, for $\nu_B > 0$, we observe a voltage decrease on the top edge starting from the source contact, while we measure nonzero voltages on the bottom edge contacts, increasing toward the source. In that configuration, from the effective Hall bar's perspective, edge channels from devices A and B have opposite chiralities, enabling equilibration in the intermediate contacts.

These observations can be all captured with a simple approach for chiral edge currents: The current emitted in one IQH channel from contact k is $e^2 V_k/h$. We assume that ideal equilibration occurs in each intermediate metallic contact and that propagation in between contacts, beyond negligible bulk leakage, is fully ballistic, insofar as it does not suffer from local (i.e., microscopic) equilibration. This last assumption is well satisfied in practice, because of the physical separation between channels of opposite chirality. Current conservation at contact k, t leads to $(\nu_A + \nu_B)V_{k,t} = \nu_A V_{k-1,t} + \nu_B V_{k+1,t}$, with $V_{N+1} = 0$ for the drain contact. We obtain the potential at each contact k on the top edge when $\nu_A \neq \nu_B$:

$$V_{k,t} = \frac{1 - \exp\left[-(N_t + 1 - k)\log\left(\nu_A/\nu_B\right)\right]}{1 - \exp\left[-(N_t + 1)\log\left(\nu_A/\nu_B\right)\right]} V_0, \qquad (1)$$

with V_0 the source voltage [27]. The same result is derived for voltages on the N_b bottom edge contacts, up to a swap between ν_A and ν_B. According to Eq. (1), for $\nu_B \neq \nu_A$, the voltage drop along the edge presents an exponential profile, highlighting a characteristic dimensionless equilibration distance $\delta = 1/|\log(\nu_A/\nu_B)|$ that should be compared with the effective edge length N_t.

This exponential profile is clearly observed in the data: Figure 2 shows voltages measured at the source and all floating contacts, for two different measurement configurations. In the first "asymmetric" configuration [Fig. 2(a)], all the contacts are located on the top effective edge ($N_t = 7, N_b = 0$), so that equilibration only occurs on the top edge and can be probed over a large number of contacts. For $(\nu_A, \nu_B) = (6, 0)$

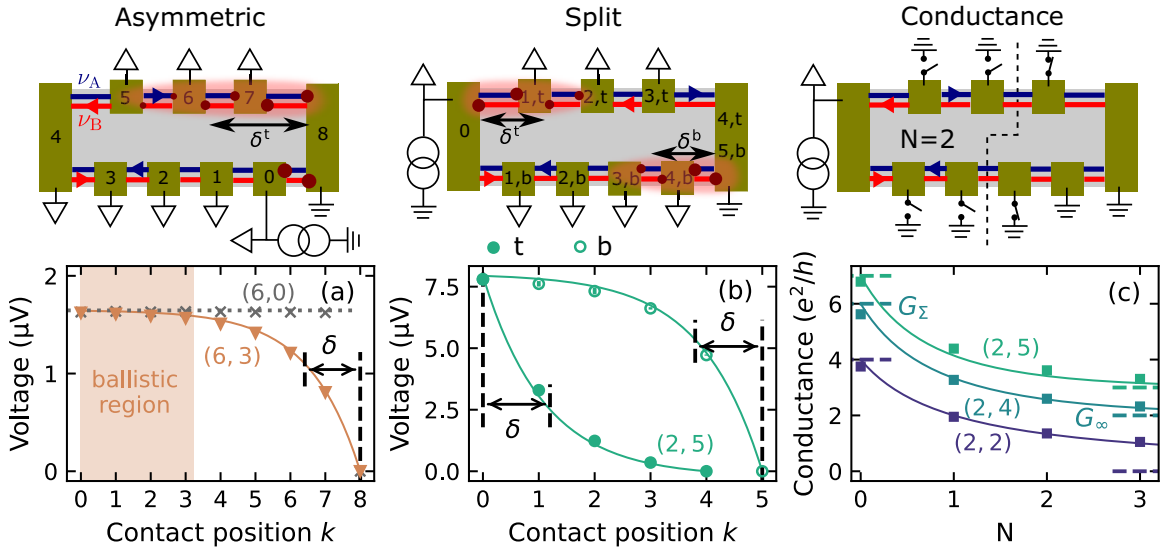

FIG. 2. (a) Sketch of the asymmetric configuration and corresponding voltage drop V_k measurements for $\nu_A = 6$, and $\nu_B = 0$ (gray crosses) and 3 (orange triangles), for an injected current amplitude $I_0 \approx 0.38$ nA. (b) Sketch of the split configuration and corresponding voltage drop measurements or $\nu_A = 2$ and $\nu_B = 5$, with injected current amplitude $I_0 \approx 0.96$ nA. Open (resp. filled) dots correspond to bottom (resp. top) edge contacts. Solid lines in both panels are applications of Eq. (1) for corresponding edges and bulk filling factors, and the dotted line in panel (a) is a guide for the eye at constant V_k. (c) Two-point conductance configuration and measurements (square symbols) for ($\nu_A = 2$, $\nu_B = 2, 4, 5$), obtained when adding pairs of grounds on each side, while keeping the bottom rightmost contact grounded to keep a symmetric configuration. Solid lines are applications of Eq. (2). Dashed lines represent the limit values of zero (G_Σ) and full (G_∞) equilibration.

(no counterpropagating channel), the voltage stays constant over the whole top edge up to the drain. For $\nu_B > 0$, e.g., the (6, 3) case represented in Fig. 2(a), the voltage remains constant and equal to that of the source contact, until a drop occurs within the last few contacts before the drain. This drop corresponds to energy dissipation over a portion of the edge, highlighted as a "hot spot" in red in Figs. 2(a) and 2(b). The measured voltage profile is exactly matched by Eq. (1), particularly the exponential dependence parametrized by the dimensionless length δ.

In the second, "split" configuration, $N_t = 3$ contacts are located on the top edge and $N_b = 4$ on the bottom edge, allowing probing the two edges independently. Figure 2(b) shows both voltage profiles for the (2, 5) case (where $\nu_A < \nu_B$), in excellent agreement with Eq. (1). On the top edge (where more channels come from the drain at zero potential than from the injection contact), the voltage rapidly drops to zero over the expected length δ. Contrarily, on the bottom edge, the voltage remains close to V_0, only dropping close to the drain over the same length δ. Therefore, the voltage profile on a given edge (saturation value and drop region) is dictated by its dominant chirality. Furthermore, it signals a ballistic behavior outside of the voltage drop region, when the effective edge length (the number of contacts) exceeds a few δ, as shown in Fig. 2(a). This is qualitatively reminiscent of dissipation in a standard QH system, where the voltage along a given chiral edge channel is constant, and only drops at the downstream contact, with a fully localized hot spot. Thus, we use hereafter the term "downstream" to indicate the end contact (source or drain) closer to which the voltage drop occurs for a given edge. We also denote ΔV_{end} by the voltage drop between the last floating contact and the downstream contact.

In addition to the voltage profile measurements, we probe the length dependence of the two-point conductance of the effective Hall bar. In this configuration [see Fig. 2(c)], the bottom contact closest to the drain is grounded to obtain a fully symmetric device. We change the sample's effective length by successively grounding pairs of contacts facing each other, starting from the drain side, thus leaving N pairs of floating contacts between the source and the grounded contacts. $N = 0$ corresponds to all contacts grounded apart from the injection one (and thus no equilibration), while $N = 3$ corresponds to none grounded except the bottom one closest to drain. The conductance in this configuration can be calculated from Eq. (1), for $\nu_A \neq \nu_B$:

$$G_{2w} = G_\infty \coth\left[\frac{N+1}{2}|\log(\nu_A/\nu_B)|\right]. \tag{2}$$

This expression also involves the characteristic length $\delta = 1/|\log(\nu_A/\nu_B)|$ and shows an exponential convergence to the equilibrated value $G_\infty = |\nu_A - \nu_B|e^2/h$ for large samples (i.e., $N \gg \delta$).

The measured conductances are displayed in Fig. 2(c) for $\nu_A = 2$ and $\nu_B = 2, 4, 5$, showing an excellent agreement with Eq. (2). We observe a clear decrease of conductance with the number N of intermediate contacts, from a value close to $G_\Sigma = (\nu_A + \nu_B)e^2/h$, which corresponds to decoupled channels at $N = 0$. Conductances are close to G_∞ already at $N = 3$. For the singular case $\nu_A = \nu_B$, the conductance slowly decreases and remains substantially above $G_\infty = 0$ at $N = 3$, and is well matched by the corresponding formula $G_{2w} = G_\Sigma/(N + 1)$ (see the Supplemental Material [27]).

The divergence of δ translates as a voltage profile that approaches the linear trend as $\nu_B \to \nu_A$ and becomes linear for the singular case $\nu_B = \nu_A$: $V_{k,\gamma=t,b} = V_0(N_\gamma + 1 - k)/$

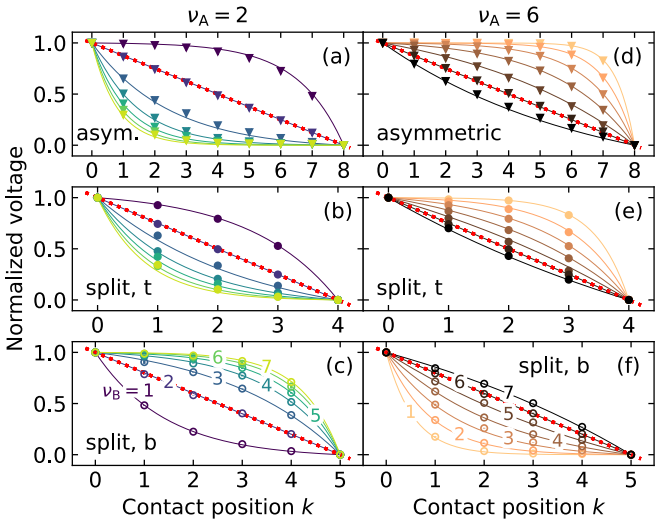

FIG. 3. Normalized voltage profiles V_k/V_0 for all ν_B values at $\nu_A = 2$ [panels (a)–(c)] and 6 [panels (d)–(f)]. Solid lines are derived from the scattering approach. Linear profiles are singled out for $\nu_A = \nu_B$ (red dotted lines).

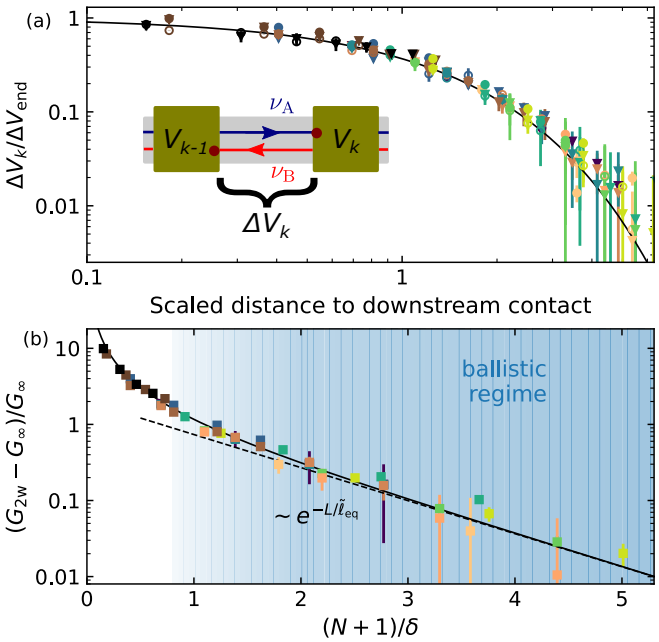

FIG. 4. (a) Voltage drops between successive contacts, normalized to the maximum voltage drop ΔV_{end}, as a function of λ/δ, the distance to the downstream contact normalized to the equilibration distance (see text). Solid line: $e^{-\lambda/\delta}$. (b) Normalized two-point conductance of the effective Hall bar in the "conductance" configuration, as a function of the scaled effective bar's length. Solid line: application of Eq. (2). The dashed line corresponds to the asymptotic limit of a ballistic ($L \gg \tilde{\ell}_{eq}$) regime, with N identified to be L/ℓ_{eq}.

$(N_\gamma + 1)$, as shown in Figs. 3(a)–(f). This corresponds to a transition to a diffusive, Ohmic regime, with a hot spot that is delocalized over the whole edge, since all voltage drops between successive contacts have the same value $-V_0/(N_\gamma + 1)$ independent of their position. This also appears in the conductance: for $\nu_A = \nu_B$, we have $G_{2w} = 2\nu_A e^2/(N+1)h$, which is confirmed experimentally through the slow, algebraic convergence of the (2, 2) conductance to zero [Fig. 2(c)].

Our results highlight universal behaviors for both voltage profiles and conductance. For $\nu_A \neq \nu_B$, the potential difference between counterpropagating channels is given by the voltage difference between successive contacts, which can be written, following Eq. (1), as $\Delta V_{k,\gamma} \equiv V_{k,\gamma} - V_{k-1,\gamma} = e^{-\lambda/\delta}\Delta V_{end,\gamma}$ ($\lambda = k$ or $N_\gamma + 1 - k$ depending on the dominant chirality on the considered edge). Therefore, equilibration is ensured for distances to downstream contact $\lambda \gg \delta$, where $\Delta V_k \approx 0$. When λ is rescaled to the equilibration distance δ, all voltage drops should collapse on a single curve and fall exponentially to zero. This is shown clearly in Fig. 4(a) for all the data presented in Fig. 3 (colors correspond to the filling factor combinations of Fig. 3).

This rescaling suggests a correspondence between our experiment and a sample with counterpropagating channels experiencing charge equilibration over a continuous edge [14–16]. Indeed, the number of Landauer reservoirs may be mapped to a continuous edge's length in units of is bare equilibration length, $N \equiv L/\ell_{eq}$. This analogy is strengthened by the similarity between Eq. (2) and the conductance of a continuous edge sample as a function of its length L in the limit of $L \gg \ell_{eq}$ [6,17]. As shown in Fig. 4(b), all reduced conductance data (see the Supplemental Material [27] for the full conductance datasets for $\nu_A = (2, 6)$ and $\nu_B = 1 \leftrightarrow 7$) $(G_{2w} - G_\infty)/G_\infty$ collapse on a single curve $\coth(x/2) - 1$, with $x = (N+1)/\delta$. For an effectively large sample, i.e., $N \gg \delta$, G_{2w} converges exponentially toward its equilibrated value G_∞, i.e., $(G_{2w} - G_\infty)/G_\infty \sim e^{-N/\delta} \equiv e^{-L/\tilde{\ell}_{eq}}$. Here we have operated a discrete-to-continuum correspondence, with $\tilde{\ell}_{eq} = \ell_{eq}/|\log(\nu_A/\nu_B)|$ the *effective* equilibration length that absorbs the contribution from filling factors measured in our experiment.

We now discuss the relation with equilibration models used for hole-conjugate states [5,6,9,11,14], particularly $\nu = 2/3$, in which charge transport exemplifies the $\nu_A \neq \nu_B$ case. In these models, the potential difference between counterpropagating edges drives interchannel charge tunneling, leading to equilibration over an effective length $\ell_{eq}/|\nu_A^{-1} - \nu_B^{-1}|$ [10,14], with ℓ_{eq} the bare equilibration length that is usually obtained in the Lüttinger liquid framework [6,17]. Our definition of $\tilde{\ell}_{eq}$ differs from this one, because the fundamentally different equilibration mechanisms are at play (interedge tunneling vs reservoir redistribution). However, in the critical regime $\nu_A \to \nu_B$, both definitions lead to the same divergence $\delta \sim 1/|\nu_A - \nu_B|$. In the diffusive case $\nu_A = \nu_B$, the two-point conductance in the macroscopic limit $L \gg \ell_{eq}$ behaves according to a universal Ohmic scaling law, decaying algebraically: $G_{2w} \propto 1/L$ [see Fig. 2(c)], irrespective of the microscopic mechanism of equilibration [5,11,12,27]. This is reminiscent of the Ohmic deviations to quantized transport observed in QSH samples [21], where the resistance scales roughly linearly with the sample's length for large samples, and analogous to the transport of heat for the disordered $\nu = 2/3$ edge, where thermal conductances are equal for charged and neutral modes, leading to diffusive signatures in noise while charge transport remains ballistic [7,9,10,17,18,28,29]. In that respect, $\nu = 2/3$ is formally equivalent to the cases (2, 6) and (6, 2) that

we study for charge, and would be equivalent to (2, 2) or (6, 6) for heat transport.

In conclusion, our experiment explores the transition between an effective ballistic edge transport (despite the presence of counterpropagating edge states) and a critical, scale-invariant diffusive regime. It conceptual simplicity makes it applicable to a large variety of systems with counterpropagating edge channels: Beyond hole-conjugate fractional and QSH states, it also encompasses the recent observation of robust quantization to the equilibrated value for the valley-polarized $\nu = -2$ state in PbSnSe Dirac systems [30]. A possible extension of this work is the investigation of the heat flow in such systems via noise measurements, e.g., to witness charge-heat separation with several fractional states, or when adding interactions, as in the case of heat Coulomb blockade [31–33].

We thank D. C. Glattli, P. Joyez, and C. Mora for helpful discussions. This work was funded by the ERC (ERC-2018-STG *QUAHQ*), by the "Investissements d'Avenir" LabEx PALM (ANR-10-LABX-0039-PALM), and by the Region Ile de France through the DIM QUANTIP. O.M. acknowledges funding from the ANR (ANR-23-CE47-0002 CRAQUANT). K.W. and T.T. acknowledge support from the JSPS KAKENHI (Grants No. 21H05233 and No. 23H02052), the CREST (JPMJCR24A5), JST and World Premier International Research Center Initiative (WPI), MEXT, Japan.

The authors declare no competing interests.

Data availability. The data that support the findings of this Letter are openly available in the following repository [34].

[1] I. Neder, M. Heiblum, Y. Levinson, D. Mahalu, and V. Umansky, Unexpected behavior in a two-path electron interferometer, Phys. Rev. Lett. **96**, 016804 (2006).

[2] H. le Sueur, C. Altimiras, U. Gennser, A. Cavanna, D. Mailly, and F. Pierre, Energy relaxation in the integer quantum Hall regime, Phys. Rev. Lett. **105**, 056803 (2010).

[3] M. König, S. Wiedmann, C. Brüne, A. Roth, H. Buhmann, L. W. Molenkamp, X.-L. Qi, and S.-C. Zhang, Quantum spin Hall insulator state in HgTe quantum wells, Science **318**, 766 (2007).

[4] A. H. MacDonald, Edge states in the fractional-quantum-Hall-effect regime, Phys. Rev. Lett. **64**, 220 (1990).

[5] C. L. Kane, M. P. A. Fisher, and J. Polchinski, Randomness at the edge: Theory of quantum Hall transport at filling $\nu = 2/3$, Phys. Rev. Lett. **72**, 4129 (1994).

[6] I. Protopopov, Y. Gefen, and A. Mirlin, Transport in a disordered $\nu = 2/3$ fractional quantum Hall junction, Ann. Phys. **385**, 287 (2017).

[7] C. Nosiglia, J. Park, B. Rosenow, and Y. Gefen, Incoherent transport on the $\nu = 2/3$ quantum Hall edge, Phys. Rev. B **98**, 115408 (2018).

[8] J. Park, A. D. Mirlin, B. Rosenow, and Y. Gefen, Noise on complex quantum Hall edges: Chiral anomaly and heat diffusion, Phys. Rev. B **99**, 161302 (2019).

[9] C. Spånslätt, J. Park, Y. Gefen, and A. D. Mirlin, Topological classification of shot noise on fractional quantum Hall edges, Phys. Rev. Lett. **123**, 137701 (2019).

[10] C. Spånslätt, J. Park, Y. Gefen, and A. D. Mirlin, Conductance plateaus and shot noise in fractional quantum Hall point contacts, Phys. Rev. B **101**, 075308 (2020).

[11] T. Fujisawa and C. Lin, Plasmon modes of coupled quantum Hall edge channels in the presence of disorder-induced tunneling, Phys. Rev. B **103**, 165302 (2021).

[12] D. C. Glattli, C. Boudet, A. De, and P. Roulleau, Revisiting the physics of hole-conjugate fractional quantum Hall channels, Phys. Rev. Res. **7**, 043026 (2025).

[13] A. Bid, N. Ofek, H. Inoue, M. Heiblum, C. L. Kane, V. Umansky, and D. Mahalu, Observation of neutral modes in the fractional quantum Hall regime, Nature (London) **466**, 585 (2010).

[14] C. Lin, R. Eguchi, M. Hashisaka, T. Akiho, K. Muraki, and T. Fujisawa, Charge equilibration in integer and fractional quantum Hall edge channels in a generalized Hall-bar device, Phys. Rev. B **99**, 195304 (2019).

[15] Y. Cohen, Y. Ronen, W. Yang, D. Banitt, J. Park, M. Heiblum, A. D. Mirlin, Y. Gefen, and V. Umansky, Synthesizing a $\nu = 2/3$ fractional quantum Hall effect edge state from counterpropagating $\nu = 1$ and $\nu = 1/3$ states, Nat. Commun. **10**, 1920 (2019).

[16] F. Lafont, A. Rosenblatt, M. Heiblum, and V. Umansky, Counter-propagating charge transport in the quantum Hall effect regime, Science **363**, 54 (2019).

[17] S. K. Srivastav, R. Kumar, C. Spånslätt, K. Watanabe, T. Taniguchi, A. D. Mirlin, Y. Gefen, and A. Das, Vanishing thermal equilibration for hole-conjugate fractional quantum Hall states in graphene, Phys. Rev. Lett. **126**, 216803 (2021).

[18] R. A. Melcer, B. Dutta, C. Spånslätt, J. Park, A. D. Mirlin, and V. Umansky, Absent thermal equilibration on fractional quantum Hall edges over macroscopic scale, Nat. Commun. **13**, 376 (2022).

[19] A. Roth, C. Brüne, H. Buhmann, L. W. Molenkamp, J. Maciejko, X.-L. Qi, and S.-C. Zhang, Nonlocal transport in the quantum spin Hall state, Science **325**, 294 (2009).

[20] I. Knez, R.-R. Du, and G. Sullivan, Evidence for helical edge modes in inverted InAs/GaSb quantum wells, Phys. Rev. Lett. **107**, 136603 (2011).

[21] S. Wu, V. Fatemi, Q. D. Gibson, K. Watanabe, T. Taniguchi, R. J. Cava, and P. Jarillo-Herrero, Observation of the quantum spin Hall effect up to 100 kelvin in a monolayer crystal, Science **359**, 76 (2018).

[22] L. Veyrat, C. Déprez, A. Coissard, X. Li, F. Gay, K. Watanabe, T. Taniguchi, Z. Han, B. A. Piot, H. Sellier, and B. Sacépé, Helical quantum Hall phase in graphene on $SrTiO_3$, Science **367**, 781 (2020).

[23] K. Kang, B. Shen, Y. Qiu, Y. Zeng, Z. Xia, K. Watanabe, T. Taniguchi, J. Shan, and K. F. Mak, Evidence of the fractional quantum spin Hall effect in moiré $MoTe_2$, Nature (London) **628**, 522 (2024).

[24] B. Yang, B. Bhujel, D. G. Chica, E. J. Telford, X. Roy, F. Ibrahim, M. Chshiev, M. Cosset-Chéneau, and B. J. van Wees,

Electrostatically controlled spin polarization in Graphene-CrSBr magnetic proximity heterostructures, Nat. Commun. **15**, 4459 (2024).

[25] M. Banerjee, M. Heiblum, A. Rosenblatt, Y. Oreg, D. E. Feldman, A. Stern, and V. Umansky, Observed quantization of anyonic heat flow, Nature (London) **545**, 75 (2017).

[26] C. R. Dean, A. F. Young, I. Meric, C. Lee, L. Wang, S. Sorgenfrei, K. Watanabe, T. Taniguchi, P. Kim, K. L. Shepard, and J. Hone, Boron nitride substrates for high-quality graphene electronics, Nat. Nanotechnol. **5**, 722 (2010).

[27] See Supplemental Material at http://link.aps.org/supplemental/10.1103/3d25-wpth for details on the sample fabrication, derivation of the voltage profiles, additional data in both integer and fractional QH regimes, and theoretical comparison between our approach and transfer matrix descriptions of the $\nu - 2/3$ edge.

[28] C. L. Kane and M. P. A. Fisher, Quantized thermal transport in the fractional quantum Hall effect, Phys. Rev. B **55**, 15832 (1997).

[29] M. Hashisaka, T. Ito, T. Akiho, S. Sasaki, N. Kumada, N. Shibata, and K. Muraki, Coherent-incoherent crossover of charge and neutral mode transport as evidence for the disorder-dominated fractional edge phase, Phys. Rev. X **13**, 031024 (2023).

[30] G. Krizman, J. Bermejo-Ortiz, T. Zakusylo, M. Hajlaoui, T. Takashiro, M. Rosmus, N. Olszowska, J. J. Kołodziej, G. Bauer, Y. Guldner, G. Springholz, and L.-A. de Vaulchier, Valley-polarized quantum Hall phase in a strain-controlled Dirac system, Phys. Rev. Lett. **132**, 166601 (2024).

[31] E. Sivre, A. Anthore, F. D. Parmentier, A. Cavanna, U. Gennser, A. Ouerghi, Y. Jin, and F. Pierre, Heat Coulomb blockade of one ballistic channel, Nat. Phys. **14**, 145 (2018).

[32] F. Stäbler and E. Sukhorukov, Mesoscopic heat multiplier and fractionalizer, Phys. Rev. B **108**, 235405 (2023).

[33] F. Stäbler, A. Gadiaga, and E. V. Sukhorukov, Giant heat flux effect in non-chiral transmission lines, Phys. Rev. Res. **7**, 033228 (2025).

[34] https://doi.org/10.5281/zenodo.15538630.